

Deep Pulse-Signal Magnification for remote Heart Rate Estimation in Compressed Videos

Joaquim Comas¹, Adrià Ruiz², Federico Sukno¹

¹ Department of Information and Communication Technologies, Pompeu Fabra University, Barcelona, Spain

² Seedtag, Madrid, Spain

Abstract—Recent advancements in remote heart rate measurement (rPPG), motivated by data-driven approaches, have significantly improved accuracy. However, certain challenges, such as video compression, still remain: recovering the rPPG signal from highly compressed videos is particularly complex. Although several studies have highlighted the difficulties and impact of video compression for this, effective solutions remain limited. In this paper, we present a novel approach to address the impact of video compression on rPPG estimation, which leverages a pulse-signal magnification transformation to adapt compressed videos to an uncompressed data domain in which the rPPG signal is magnified. We validate the effectiveness of our model by exhaustive evaluations on two publicly available datasets, UCLA-rPPG and UBFC-rPPG, employing both intra- and cross-database performance at several compression rates. Additionally, we assess the robustness of our approach on two additional highly compressed and widely-used datasets, MAHNOB-HCI and COHFACE, which reveal outstanding heart rate estimation results.

Index Terms—rPPG, video compression, pulse-signal magnification, two-stage framework.

I. INTRODUCTION

Recently, the research community has shown increasing interest in the camera-based measurement of human physiological signals. These vital signs, including heart rate (HR), heart rate variability (HRV), respiration rate (RR), oxygen saturation (SpO₂), and blood volume pulse (BVP) are essential for evaluating individuals' physical and mental state and have numerous potential applications [1], [24], [43]. The advancements in multimedia technology have made many of these potential applications feasible, and have significantly impacted various industries such as education, entertainment, advertising, and healthcare. Thanks to current network connections, smartphones, and other multimedia devices, multimedia content can be accessed or shared effortlessly. Nevertheless, in practical scenarios, the transmission of vast amounts of content would not be viable without the use of video compression.

While significant progress has been made in the study of remote physiological signal sensing, its application to compressed videos remains challenging. McDuff et al. [30] were among the first to demonstrate the impact of video compression, noting a significant reduction in the rPPG signal-to-noise ratio (SNR), even before human observers perceive a decrease in visual quality. Thus, it was found that even mild compression affects the recovery of the rPPG signal and, through this, the accuracy of derived estimates, such as HR or RR.

Prior to the above study, many researchers had overlooked the negative effects of video compression on the extraction of camera-based biosignals, particularly in the acquisition of facial videos. Since then, several other works [3], [34], [49], [67] have contributed to demonstrating additional effects of video compression on automatic rPPG analysis, such as the effect of video resolution [49], the heterogeneous impact of compression for different color channels [67], or the greater impact of temporal compression with respect to chroma and spatial compression on the quality of the recovered rPPG signal [42]. More details on these and other studies about the impact of video compression can be found in Section II-C.

Unfortunately, to date, rather few solutions have been proposed to address the challenges arising from video compression in rPPG estimation, which can be broadly divided into three categories: 1) methods that propose to modify the recording conditions or the encoding algorithm [66], [67]; 2) methods that propose to avoid a mismatch between the compression rates of training and test sets [34], [36]; 3) methods which try to reverse the damage introduced by the compressor [62] (details in Section II-D).

In practice, the first category is of limited scope because it only applies to scenarios where videos are recorded specifically for rPPG estimation purposes. The second category is more widely applicable since it only requires finding a training dataset that matches the compression of the data being targeted; however, its success has been modest, yielding results that are still largely affected by the amount of compression [34]. Thus, the most promising path so far has been the third category, where the most relevant approach was presented by Yu et al. [62], based on an enhancement generator (STVEN) cascaded with a spatiotemporal convolutional network (rPPGNet) to recover the rPPG signal. The enhancement generator is framed within the idea of video quality enhancement (VQE) [9], [64], which requires significant computational resources due to the large amount of data involved in restoring the high-frequency details lost due to video compression. Nevertheless, this is mainly due to the tendency of VQE methods to prioritize visual quality enhancement, which, as we will show, is not strictly needed to recover the rPPG signal.

A. Contribution

In this work, we propose a novel deep learning framework to mitigate the impact of video compression on rPPG recovery that departs from the objective of Visual Quality Enhance-

ment and focuses, instead, on enhancing only the information required to allow proper recovery of the rPPG signal. To this end, we present a training methodology involving two deep neural networks: (i) The rPPG estimator network trained on uncompressed videos that attempts to recover the rPPG signal. (ii) The Pulse-Signal Magnification network, which adapts compressed facial videos to a pulse-signal magnified video domain in which the effects of the blood volume pulse are amplified, facilitating the rPPG extraction by the rPPG estimator network even in highly compressed scenarios. We present an effective two-stage optimization procedure for both networks in order to achieve higher generalization ability of our system in cases where uncompressed video data is scarce. Finally, we evaluate our experiments on two publicly available uncompressed datasets, UCLA-rPPG and UBFC-rPPG, and demonstrate its robustness and generalization through intra- and cross-dataset evaluation on two highly compressed public datasets, MAHNOB-HCI and COHFACE.

The remainder of this paper is organized as follows: firstly, in Section II, we conduct a comprehensive review of the effects of video compression on rPPG estimation, the available solutions, and the prevalence of video compression in existing rPPG datasets. The proposed approach is presented in Section III, while experimental results are provided in Section IV. Section V summarizes our findings and conclusions.

II. RELATED WORK

A. Camera-based Physiological measurement

Since Takano et al. [52] and Verkruyse et al. [56] showed the feasibility of measuring HR remotely from facial videos, many researchers have proposed different methods to recover physiological data. Among them, some works consider regions of interest using various techniques, including Blind Source Separation [20], [40], [41], Normalized Least Mean Squares [23] or self-adaptive matrix completion [55]. In contrast, other works rely on the skin optical reflection model by projecting all RGB skin pixel channels into an optimized subspace mitigating motion artifacts [8], [57].

Recently, deep learning-based methods [19], [27], [35], [39], [50], [62] have outperformed conventional methods and achieved state-of-the-art performance in estimating vital signs from facial videos. Some of these methods leverage prior knowledge learned from traditional methods and combine it with Convolutional Neural Networks (CNNs) to exploit more sophisticated features [31], [33], [46]. Some recent works [19], [26] have explored unsupervised approaches using meta-learning, showing improved generalization in out-of-distribution cases. On the other hand, some other researchers have aimed at fully end-to-end approaches [4], [39], [61]. Unlike previous methods, end-to-end models utilize facial videos as input to directly predict the rPPG signal. Recently, unsupervised techniques have gained traction in end-to-end approaches, with transformer-based models like Physformer [63] and EfficientPhys [25] leading the way in leveraging long-range spatiotemporal features. Nevertheless, these models are currently not optimized for computational efficiency, making them unsuitable for deployment on mobile devices. Further-

more, while they show promise, they may not yet demonstrate a significant performance advantage over CNN-based models [25]. To tackle this challenge, in this paper, we explore a widely recognized architecture inspired by [62] jointly with [5] to address the impact of video compression on rPPG extraction while also controlling its computational cost.

B. Video-compression in existing rPPG datasets

Several datasets have been collected for camera-based physiological sensing in recent years, addressing factors such as head movements, illumination conditions, and facial skin diversity. However, the effect of video compression in the recovery of rPPG signals has been largely overlooked, since most of the existing datasets are already overcompressed [14], [45], [65]. Although a few uncompressed datasets have emerged [2], [10], [51], not all of them are available to the public and have limited sample sizes, making it challenging to propose effective solutions, particularly with deep learning-based approaches.

Table I summarizes existing rPPG datasets and different information related to video compression including format, camera specifications, and approximate video quality from facial video in terms of bitrate¹. Although we can distinguish different content formats in the existing rPPG datasets, the majority of them are stored using three standard compression codecs: MPEG-4 Video Part 2 (MPEG-4), Advanced Video Coding (H.264) and Motion JPEG (MJPG).

MPEG-4 and H.264 are video compression standards that use block-wise motion compensation. H.264 is an improved version of MPEG-4, providing better compression due to variable block-size segmentation, optimal discrete cosine transform (DCT), and enhanced inter-frame prediction. While H.264 is the most common format, MPEG-4 is used in some datasets, including COHFACE [14], OBF [22], and CMU [7]. VIPL-HR [32] and UBFC-Phys [44] use the MJPG codec, which compresses each frame individually using JPEG compression, minimizing inter-frame compression's impact on HR estimation [32]. However, the JPEG codec's quantization stage makes it challenging to explore compression rPPG solutions. In contrast, uncompressed datasets have more diversity regarding codec format, with some storing raw data in image files using lossless formats such as PNG, BMP, or Bayer format (e.g., PURE [51], or MR-NIRP [28]), and others using uncompressed video formats, including YUV420, RV32, and RGBA format (e.g., ECG-Fitness [50] or UBFC-rPPG [2]).

Regarding video quality, a significant average bitrate difference is exhibited between non-compressed and highly compressed datasets, such as UCLA-rPPG [58] with 295 Mb/s and COHFACE [14] with 0.250 Mb/s. In this case, both datasets used the same camera resolution, but the effects of video compression yield a notable difference in video quality. Also, as noted by Špetlík et al. [49], the encoding standard alone cannot determine video quality. Despite the effects of these video compression codecs, other factors, such as the pixel format or the camera resolution, must be considered in the bitrate computation. The VicarPPG and MAHNOB-HCI

¹To collect the video information from the different datasets, we contacted the authors of each dataset and utilized the open-source FFmpeg ffprobe tool: <https://ffmpeg.org/ffprobe.html>

datasets use H.264 encoding but with different camera settings resulting in highly different average bitrates. VicarPPG has a bitrate of 34 Mb/s, while MAHNOB-HCI has a bitrate of 4.20 Mb/s. This means that MAHNOB-HCI has approximately 8.5 times lower quality than VicarPPG.

C. Influence of video compression on rPPG estimation

Video compression techniques optimize visual quality by removing imperceptible information from the human eye. However, it may also remove subtle color variations that are important for inferring rPPG signals from the video. Hanfland et al. [13] was the first to show the influence of video compression on iPPG signal extraction. They compressed raw videos using Motion JPEG, MPEG-4, and Motion JPEG 2000 codecs and computed the time-domain correlation between the videos and extracted signals. Although they stated that the iPPG signal was preserved, the overall quality was altered by the compressions. McDuff et al. [30] analyzed the impact of video compression on rPPG signal quality by testing two compression standards, H.264 and H.265, at different compression ratios. They found noticeable degradation of the rPPG signal even with low-level compression ratios and concluded that videos with a bit rate of 10 Mb/s maintained an rPPG signal with reasonable SNR. They suggested using H.265 instead of H.264 codec, especially for videos with large movement variations. Similarly to McDuff et al., [30], Cerina et al. [3] analyzed the impact of frame rate and video compression on remote pulse-rate variability (PRV) using a lossless (FFV1) and lossy format (H.264) at two compression ratios. They observed a notable trade-off between PRV quality and storage size in FFV1 format, while H.264 showed higher degradation in heart rate variability, dependent on peak detection accuracy.

Other studies have further explored the impact of video encoding on camera physiological measurements. One study by Špetlík et al. [49] identified errors in the acquisition stage and conducted an experiment similar to [30] to demonstrate the degradation of rPPG signal SNR at various compression ratios using H.264 encoding. They found that lower resolutions had a more negative impact on the recovered signal SNR and emphasized the negative effects of chroma subsampling, common in web camera hardware settings. Another study [42] analyzed the effects of different factors in video compression, finding that inter-frame compression was more damaging than intra-compression or chroma subsampling. Zhao et al. [67] found that high compression levels affected blue and red color channels the most in terms of amplitude degradation, high-frequency noise, and trace discontinuity. Nowara et al. [36] extended the study of video compression on rPPG recovery to evaluate its effects on large motion cases and the impact of skin diversity in compressed videos.

Some works like Niu et al. [32], and Gudi et al. [12] investigated the impact of video compression on the development of rPPG datasets, as described in the previous Section II-B. The first one compressed the raw data using five different video codecs: MJPG, FMP4, DIVX, PIM1, and H264, and evaluated the accuracy of HR estimation. Their results determined that the MJPG codec provided an appropriate balance between data reduction and preservation of rPPG signals. Instead, the second

one explored the trade-off between rPPG accuracy and video size/bitrate in the PURE dataset. They used different lossy (VP9, H.264, H.265, MJPG, MPEG-4) and lossless (FFV1, HuffYUV) video codecs at varying bitrates. They concluded that H.265 and FFV1 were the most efficient codecs for preserving rPPG accuracy and storage, respectively.

Our findings, discussed in Section IV-C, align with these prior studies that highlight the negative effects of video compression on the retrieval of rPPG signals. However, in addition to validating these observations, we introduce a novel approach outlined in Section III, that effectively mitigates the adverse effects induced by video compression. One of the crucial choices in the design of the proposed approach is the usage of uncompressed datasets. As mentioned earlier, recovering the rPPG signal from compressed data leads to suboptimal results with a degraded signal due to compression. To maximize the search for an optimal mapping between compressed and uncompressed videos, and to magnify the pulse signal from the facial region, it is essential to use uncompressed data.

D. rPPG solutions for compressed facial videos

Several studies have evaluated the effects of compression on rPPG measurements, but few have proposed effective solutions for extracting pulse signals from compressed videos. Zhao et al. [67] developed a single-channel pulse extraction method that only considers the green channel, as it is less affected by video compression artefacts. However, ignoring the other channels leads to suboptimal estimations as important rPPG information is neglected. Another solution proposed by Zhao et al. [66] involved designing a new video compression codec that compresses regions not involved in rPPG extraction, but this approach is not practical for already compressed videos and is challenging to standardize across all multimedia content.

Data-driven solutions have also been explored. McDuff [29] introduced a preprocessing step for deep super-resolution to restore high-frequency spatial details from low-resolution or intra-frame (spatial) compressed facial videos, but this method does not consider the adverse effects of inter-frame (temporal) compression. In contrast, Nowara et al. [34], [36] demonstrated that models trained on videos with the same compression level as the test set achieve better performance with respect to mismatched train-test compression; however, this method requires knowledge of the compression ratio of the testing videos and does not address video compression explicitly.

Finally, Yu et al. [62] presented the first enhancement method to deal with temporal compression using a video-to-video generator called STVEN and an rPPG estimator called rPPGNet. They employed a three-stage training process and multiple objective loss functions to optimize both models. The STVEN generator is firstly trained to reconstruct uncompressed videos from compressed ones and independently, the rPPGNet estimator is optimized using high-quality videos. Finally, a joint training step was performed, fixing the parameters of the rPPGNet estimator and optimizing the STVEN generator to enhance facial videos for rPPG extraction.

²The original camera pixel format was YUV422P format, but it was compressed in a lossless H.264 using a Constant Rate Factor (CRF) of 0

TABLE I: Summary of the existing camera-based physiological signal sensing databases and its specifications.

Dataset	Year	Publicly available	Camera Settings	Average Bitrate	Data Format	Subjects	Videos	Signal acquisition
MAHNOB-HCI [45]	2011	Yes	RGB camera, 780x580, 61 Hz	4.20 Mb/s	H.264	27	527	ECG, GSR, RF, ST, EEG
AFRL [10]	2014	No	RGB camera, 658x492, 30 Hz	310 Mb/s	Raw (Bayer)	25	300	ECG, BVP
PURE [51]	2014	Yes	RGB camera, 640x480, 30 Hz	222 Mb/s	Raw (PNG)	10	59	PPG, SpO2
VicarPPG [53]	2014	Yes	Webcam, 720x1280, 30 Hz	34 Mb/s	H.264	10	20	PPG
BP4D [65]	2016	No	Webcam, 1040x1392, 25 Hz	3.5 Mb/s	H.264	140	1400	PPG, RF, HR, EDA
COHFACE [14]	2017	Yes	Webcam, 640x480, 20 Hz	0.25 Mb/s	MPEG-4	40	160	PPG, RF
UBFC-rPPG [2]	2017	Yes	Webcam, 640x480, 30 Hz	215 Mb/s	Raw (RV24)	42	42	HR, PPG
OBF [22]	2018	No	RGB/NIR camera, 1920x1080, 60 Hz	20 Mb/s	MPEG-4	106	212	ECG, RF, PPG
ECG-Fitness [50]	2018	Yes	Webcam, 1920x1080, 30 Hz	745 Mb/s	Raw (YUV420)	17	204	ECG
MR-NIRP [28]	2018	Yes	RGB/NIR camera, 640 × 640, 30 Hz	590 Mb/s	Raw (Bayer)	18	37	PPG
PPF [15]	2020	Yes	Webcam, 1280x720, 50Hz	10 Mb/s	H.264	13	85	HR
VIPL-HR [33]	2020	Yes	RGB/NIR camera, 960x720, 640x480, 25-30 Hz	5.15 Mb/s	MJPEG	107	3130	HR, SpO2, PPG
MOLI-PPG [39]	2020	No	Webcam/RGB camera, 1280x720, 1920x720, 25-50 Hz	Unknown	Raw (BMP)	30	229	PPG
VicarPPG-2 [12]	2020	Yes	Webcam, 1280x720, 60 Hz	16.5 Mb/s	H.264	10	40	PPG, ECG
CMU [7]	2021	Yes	Smartphone, 25x25, 15 Hz	0.145 Mb/s	MPEG-4	140	140	HR
CameraHRV [37]	2021	Yes	RGB camera, 1920x1200, 30 Hz	1659 Mb/s	Raw (Bayer)	14	60	PPG
UBFC-Phys [44]	2021	Yes	RGB camera, 1024x1024, 35 Hz	225 Mb/s	MJPEG	56	168	PPG, EDA
DDPM [48]	2021	Yes	RGB/NIR camera, 1920 × 1080, 90 Hz	950 Mb/s	H.264 ²	86	86	PPG, SpO2, HR
UCLA-rPPG [58]	2022	Yes	RGB camera, 640x480, 30 Hz	295 Mb/s	Raw (RGBA)	98	489	PPG, HR

In contrast to Yu et al., we propose a simpler two-stage approach that improves existing HR estimation in highly compressed scenarios by focusing solely on the physiological perspective. Our Pulse-Signal Magnification Network is designed to learn a video transformation to magnify the rPPG characteristics instead of trying to reconstruct all uncompressed video details, which are unnecessary for the problem at hand and computationally more expensive.

III. METHODOLOGY

In this section, we introduce our proposed model, which is composed of the rPPG estimator and the Pulse-Signal Magnification networks. Subsequently, we detail our two-stage training procedure and finally present our optimized objective function for rPPG recovery.

A. Problem formulation

Our framework aims to extract the rPPG signal from compressed videos by utilizing a learned video transformation. This transformation aims to magnify the video signal useful for rPPG extraction, mitigated by the video compression process. It achieves this by magnifying the video signal information in the compressed video relevant to rPPG estimation.

Let $\mathbf{C}^n = [c_1^n, c_2^n, \dots, c_T^n]$ be a facial compressed video $n \in N$, where N is the total number of videos with the number of frames $t \in T$ in our training set. The corresponding rPPG ground-truth signal from the set of compressed \mathbf{C}^n is denoted as $\mathbf{y}_c^n = [y_{c,1}^n, y_{c,2}^n, \dots, y_{c,T}^n] \in \mathcal{Y}$. Given previous

definitions, we denote our compressed rPPG video dataset as $\mathcal{D}^C = [(\mathbf{C}^1, \mathbf{y}_c^1), \dots, (\mathbf{C}^N, \mathbf{y}_c^N)]$. Similarly, we assume that, during training, we have also access to the analogous set of uncompressed facial videos $\mathbf{U}^n = [u_1^n, u_2^n, \dots, u_T^n] \in \mathcal{U}$, also with their corresponding PPG ground-truth $\mathbf{y}_u^n = [y_{u,1}^n, y_{u,2}^n, \dots, y_{u,T}^n]$, forming the rPPG uncompressed dataset $\mathcal{D}^U = [(\mathbf{U}^1, \mathbf{y}_u^1), \dots, (\mathbf{U}^N, \mathbf{y}_u^N)]$. As previously mentioned, our two-stage framework involves training two neural networks: f_θ and m_ψ . The network f_θ learns the mapping from uncompressed facial video \mathcal{U} to rPPG signal \mathcal{Y} , while the network m_ψ maps the compressed RGB facial video \mathcal{C} to a new pulse-signal magnification subspace \mathcal{M} :

$$\begin{aligned} f_\theta : \mathcal{U} &\rightarrow \mathcal{Y} \\ m_\psi : \mathcal{C} &\rightarrow \mathcal{M} \end{aligned} \quad (1)$$

where θ and ψ refer to the rPPG and pulse-magnification network, respectively. Given previous definitions, our objective is to approximate the relationship between uncompressed \mathcal{U} and compressed \mathcal{C} facial videos by learning a video transformation that effectively amplifies the information related to the pulse signal that was distorted by the compression effect:

$$M^n = f_\theta(m_\psi(\mathbf{C}^n)) \in \mathcal{M}, \quad (2)$$

where M^n represents generated pulse-signal magnified video from the compressed facial video \mathbf{C}^n .

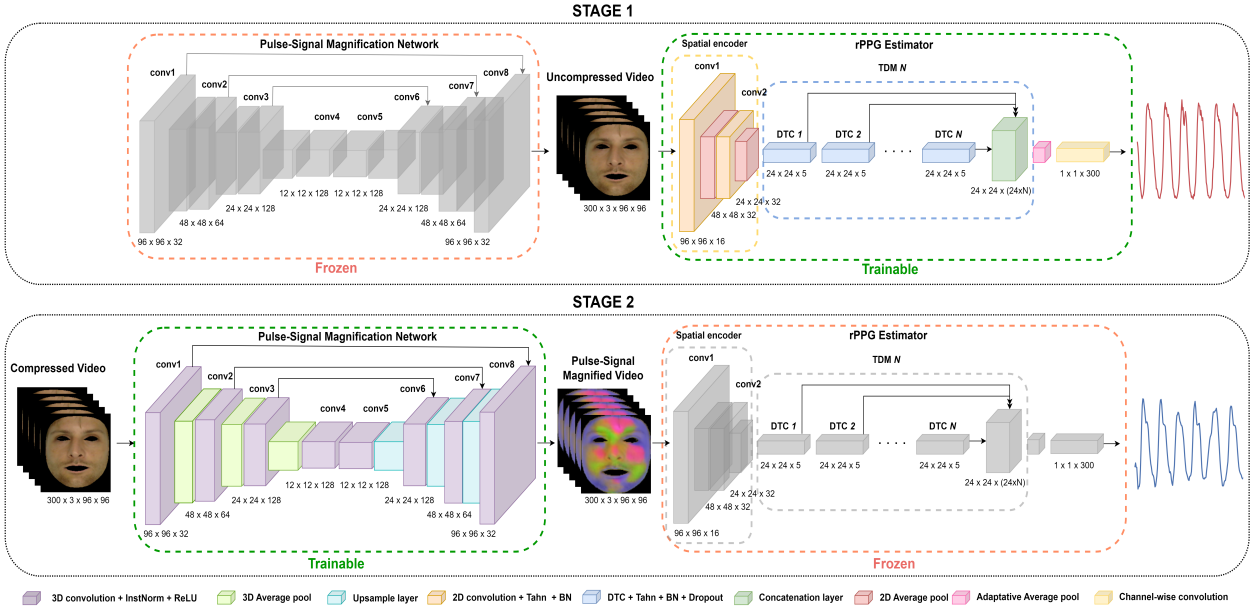


Fig. 1: Overall structure of our proposed model, which has two stages for rPPG recovery under compression. Firstly, the TDM model is trained on uncompressed data. Secondly, the Pulse-Signal Magnification network is trained on compressed data with fixed TDM model parameters.

B. Pulse-Signal and rPPG Estimator Networks Architecture

An illustration of the two networks previously described is provided in Figure 1. The rPPG estimator network f_θ is a lightweight spatiotemporal model presented in [5]. This network effectively estimates rPPG spatiotemporal features by aggregating temporal derivatives modules (TDM), emulating a Taylor series expansion. We selected this architecture because it achieves competitive results in current benchmarks while using fewer parameters than existing solutions.

The Pulse-Signal Magnification network m_ψ is an Unet-based network that learns the desired pulse-signal magnification transformation. This spatiotemporal network comprises three 3D convolutions with a $3 \times 3 \times 3$ kernel size, followed by the ReLU activation function, 3D instance normalization, and average pooling operation. We then employ two spatiotemporal convolutions in the lowest dimensionality space and reconstruct the latent space using three 3D upsampling convolutions. At each resolution level, we incorporate a skip connection to enforce the network to obtain the same facial data as the input.

C. Two-stage Training Framework

The motivation for our proposed two-stage training framework is three-fold: 1) to better handle the domain gap between compressed and uncompressed videos in the recovery of remote PPG signal by magnifying the pulse signal in the video domain, 2) to leverage a pre-trained rPPG estimator network f_θ on an uncompressed video dataset as a regularizer for the Pulse-Signal Magnification network m_ψ , and 3) to reduce the computational complexity and training time of the overall system. By decoupling the training into two stages, we can ensure that the Pulse-signal Magnification network m_ψ learns a representation that better approximates the performance of

uncompressed video format while freezing the parameters of the rPPG estimator network while optimizing m_ψ provides a regularization term that helps to avoid overfitting and improves the generalization ability of the learned representation.

1) Stage I:

The first stage of the framework consists of training our f_θ as rPPG estimator from uncompressed data \mathcal{D}^u . The purpose of this stage is to obtain a pre-trained network that can estimate the PPG signal accurately from uncompressed videos, which can be used as a regularizer for the Pulse-Signal Magnification network m_ψ in the second stage. This stage is essential in addressing the domain gap between compressed and uncompressed videos, as the pre-trained rPPG estimator network f_θ can capture the signal from uncompressed videos more effectively than using compressed data. Therefore, the objective of this first stage is to optimize our f_θ network over θ parameters, such that:

$$\min_{\theta} \frac{1}{N} \sum_{n=1}^N \mathcal{L}_{\text{rPPG}}(f_{\theta}(\mathbf{U}^n), \mathbf{y}_{\mathbf{u}}^n), \quad (3)$$

where n is the index of the uncompressed video \mathbf{U}^n , $\mathbf{y}_{\mathbf{u}}^n$ the corresponding PPG ground-truth signal, and $\mathcal{L}_{\text{rPPG}}$ is the rPPG loss function that measures the difference between the estimated PPG signal and the PPG ground-truth signal, explained in Section III-D.

2) Stage II

The second stage of the framework involves training a Pulse-Signal Magnification network m_ψ to learn a desired video transformation. In a study by Nowara et al. [34], it was argued that training deep learning models with the same compression level as the testing data yields the best performance. Following this idea, the pre-trained rPPG estimator model f_θ is designed to estimate the rPPG signal from non-compressed

videos, while the Pulse-Signal Magnification network m_ψ learns to map videos in the domain of \mathcal{C} to a domain which magnifies the pulse-signal from compressed data \mathcal{D}^c to behave like non-compressed data \mathcal{D}^u , adapting the compressed level of input data to the uncompressed format guided by the knowledge from f_θ network in Stage I.

Thus, the objective of the second stage is to jointly train both networks such that the output of m_ψ is regularized by f_θ . The parameters θ of the rPPG estimator network f_θ are kept frozen during this training, meaning that only the parameters ψ of the Pulse-Signal Magnification network m_ψ are updated:

$$\min_{\psi} \frac{1}{N} \sum_{n=1}^N \mathcal{L}_{\text{rPPG}}(f_\theta(m_\psi(\mathbf{C}^n)), \mathbf{y}_c^n), \quad (4)$$

where n is the index of the compressed video \mathbf{C}^n , \mathbf{y}_c^n is the corresponding ground-truth PPG signal, and $\mathcal{L}_{\text{rPPG}}$ is the rPPG loss function. In Section IV-C, we will discuss the advantages of this two-step approach and present empirical evidence of its effectiveness in our experimental section.

D. Loss function

We utilized a combined loss function focused solely on the physiological aspect to direct the optimization of our proposed model toward improving the input video. The combined loss function comprises a temporal loss function aimed at restoring the intrinsic characteristics of the PPG waveform, and a frequency loss function, aimed at learning spectral features from the HR distribution.

For the temporal loss function, we adopted TALOS (Temporal Adaptive LOcation Shift) Loss, presented in [5] that allows training of deep learning methods invariantly to temporal offsets of the ground-truth signal, also known as Pulse Transit Time (PTT). Therefore, our $\mathcal{L}_{\text{temp}}$ can be written as:

$$\mathcal{L}_{\text{TALOS}} = \sum_{k \in K} \text{MSE}(\hat{y}_t, y_{(t-k)}) \cdot p_\theta(k|s), \quad (5)$$

where the mean square error (MSE) is computed between the predicted rPPG signal \hat{y}_t and the ground-truth PPG signal $y_{(t-k)}$ for each possible offset k and is weighted according to the learned temporal-shift probability $p_\theta(k|s)$.

For the frequency loss function, we employed the signal-to-noise ratio (SNR) loss [8] to incorporate the HR estimation task as a classification problem in the frequential domain. Therefore, our $\mathcal{L}_{\text{freq}}$ can be written as:

$$\mathcal{L}_{\text{CE}} = \text{CE}(\text{PSD}(\hat{y}_t), \text{HR}_{gt}), \quad (6)$$

where the CE is the cross-entropy loss between the $\text{PSD}(\hat{y}_t)$, which is the power spectral density computation of the predicted rPPG signal \hat{y} and the HR_{gt} , which represents the HR ground-truth value.

In summary, the overall loss function $\mathcal{L}_{\text{rPPG}}$ for both networks can be formulated as:

$$\mathcal{L}_{\text{rPPG}} = \mathcal{L}_{\text{temp}} + \lambda \cdot \mathcal{L}_{\text{freq}}, \quad (7)$$

where λ is a balancing parameter. In our experiments, we set $\lambda = 0.01$ empirically based on our preliminary experiments.

E. Constrained Pulse-Signal Magnification space

Once our loss is formalized, let us revisit the concept behind our training stage II, introduced in Section III-C2. While the problem was initially stated like a VQE framework, we do not actually target the restoration of the compressed video to its uncompressed form, since there are no video reconstruction terms in our loss function. Instead, we only target the minimization of the estimated PPG signal and the HR extracted from it, respectively, with $\mathcal{L}_{\text{TALOS}}$ and \mathcal{L}_{CE} . This does not lead to the enhancement of the *visual quality* of the transformed video, but rather to its transformation into an alternative, arbitrary domain in which the only constraints are those imposed in the aforementioned losses.

Thus, M^n is not a decompressed version of U^n , but a transformation into a latent physiological domain in which the PPG signal can be extracted with an accuracy similar to the uncompressed case, yet while starting from the compressed video input. As we shall see in the experiments, the transformed video is largely distorted in terms of visual quality, but it effectively focuses on the intensity changes that are relevant to estimate the PPG signal. Indeed, after processing the input video with our Pulse-Signal Magnification network m_ψ , the pulsatile effect on the skin becomes magnified, to the extent that it can be appreciated by the naked eye.

The above amplification is achieved through the regularization effect of the uncompressed rPPG intrinsic features learned by the rPPG estimator, f_θ . Consequently, applying the proposed two-stage framework, optimized exclusively from the rPPG perspective, yields a novel physiologically magnified video that amplifies the pulse signal, which is imperceptible to the naked eye in the input RGB domain. This pulse-signal magnification space will be further examined in Section IV-C.

IV. EXPERIMENTS

In this section, we present the four benchmark datasets utilized in our experiments and describe the implementation of our method. We will begin by examining the effect of the loss function in our model, followed by investigating the impact of video compression on rPPG recovery using our baseline model at various compression levels. Next, we will evaluate the performance of our two-stage model through intra-database and cross-database evaluations, showing its robustness to video compression. Finally, we will present a relative comparison with existing rPPG approaches on compressed benchmarks.

A. Datasets

We evaluated our approach on the following RGB video datasets.

The **UCLA-rPPG** dataset [58] comprises 489 videos from 98 subjects with diverse characteristics, including skin tones, ages, genders, and ethnicities. It was specifically curated to generate synthetic avatars for rPPG estimation. Each subject underwent five trials, with each trial lasting approximately 1 minute. The recordings were captured at a resolution of 640 x 480 pixels and 30 frames per second (FPS), in an uncompressed format, with an average bit rate of around 295 Mb/s. Synchronous gold-standard PPG and HR measurements

were collected alongside the facial videos. Due to the lack of predefined folds in this dataset, we split the data into training (80%), validation (10%), and testing (10%) sets.

The **UBFC-rPPG** [2] includes 42 RGB videos from 42 subjects. The subjects were asked to play a time-sensitive mathematical game, emulating a standard human-computer interaction scenario, to obtain varied HR during the experiment. The recorded facial videos were acquired indoors with varying sunlight and indoor illumination at 30 FPS with a webcam (Logitech C920 HD Pro) at a resolution of 640x480 in uncompressed 8-bit RGB format, with an average bit rate \approx 215 Mb/s. The bio-signals ground truth was acquired using a CMS50E transmissive pulse oximeter to record the PPG signal and heart rate with a 30 Hz sampling rate. In our experiments, we used UBFC-rPPG in a cross-dataset evaluation, where all 42 videos were used for testing.

The **COHFACE** [14] consists of 160 videos from 40 subjects, where each subject was recorded in 4 trials captured under two different lighting environments: studio and natural light. Each video was recorded with a Logitech C525 web camera at 20 FPS with a resolution of 640x480 for 1 minute and stored with heavy MPEG-4 compression, with an average bit rate \approx 0.25 Mb/s. The physiological data is recorded using Thought Technologies devices to acquire PPG and respiration ground-truth signals with a sampling rate of 256 Hz. For our comparison, we follow the preassigned standard folds defined for the dataset.

The **MAHNOB-HCI** [45] is a multimodal database originally recorded for emotion recognition and implicit tagging of multimedia content. It includes 527 facial videos from 27 participants (15 women, 12 men) with corresponding physiological signals. The videos were recorded at a resolution of 780x580 and 61 FPS, which were heavily compressed in H.264/MPEG-4 AVC compression, with an average bit rate \approx 4.20 Mb/s. Regarding the physiological data, each recording contains an electroencephalogram (EEG), galvanic skin response (GSR), electrocardiogram (ECG), temperature and respiration signals acquired with a Biosemi active II system and later downsampled to 256 Hz. Since the MAHNOB-HCI dataset was not acquired for rPPG estimation purposes, we generated HR ground truth from the ECG signal using the Bob Toolbox³ [14]. To compare fairly with previous works [4], [19], [62], we used the standard 30-second clip (frames 306 to 2135) of each video.

B. Implementation details

1) Preprocessing and training procedure

We adopt the same preprocessing stage for each dataset in all our experiments. Firstly, since our model is not attempting to solve the video compression task itself; we decided to apply a facial preprocessing segmentation to remove the background and non-skin areas adapting the Mediapipe Face Mesh⁴ model [18]. This step reduces the complexity of video compression by focusing attention on the facial skin without introducing more complexity in terms of parameters or optimization tasks.

Once the facial video is masked each video frame is resized to 96×96 pixels. The ground-truth bio-signal is preprocessed following [6] to denoise the raw PPG signal, which facilitates a better model convergence during the training procedure. We implement our model using Pytorch 1.8.0 [38] and train it on a single NVIDIA GTX1080Ti. We use sequences of 300 frames with an overlap of 10 samples and Adam optimizer during training with a learning rate of 0.0001 and weight decay of $1e-5$. In addition, when using our TALOS loss, we incorporate an extra SGD optimizer with a 0.01 learning rate to optimize the parameters θ^s of the temporal-shift distributions for each subject. Finally, the estimated HR is computed from the predicted rPPG signal using the power spectral density (PSD). Before calculating the HR value, we apply a band-pass filter with cutoff frequencies of 0.66 Hz and 3 Hz.

2) Video compression settings

To evaluate the impact of video compression rate, we adopt the methodology from [30] in developing our ablation studies on our two non-compressed datasets. To compress the data, we used the FFmpeg software and evaluated the impact of video compression using the H.264 codec at various levels. To achieve this, we utilized the Constant Rate Factor (CRF) parameter, which maintains a constant visual quality level by dynamically adjusting the bitrate based on video content complexity. The CRF values range from 0 to 51, with lower values indicating higher quality. For our ablation studies, we consider CRF values of 0, 5, 10, 15, 20, and 25 in our experiments, with 0 representing the uncompressed data.

3) Metrics and evaluation

To evaluate the HR estimation performance of the proposed model, we adopted the same metrics used in the literature, such as the mean absolute HR error (MAE), the root mean squared HR error (RMSE) and Pearson’s correlation coefficients R. For the UCLA-rPPG intra-dataset experiments, we used 300-frame sequences (10-second windowed) without overlapping for HR estimation. This approach is more challenging and informative compared to estimating HR based on the entire video sequence at once. For the remaining datasets, we computed whole-video performance to fairly compare our method to the state-of-the-art because most prior work adopts whole-video evaluation. This allows for a direct comparison of our approach to several traditional and deep learning methods.

C. Ablation studies

In Section II-B, we emphasize the importance of utilizing an uncompressed dataset for optimal results in our two-stage framework. As a result, we primarily choose the publicly available UCLA-rPPG dataset as the training dataset for our ablation studies. This dataset meets our criteria by including a substantial number of subjects with diverse skin types and being in an uncompressed format.

In this section, we present the results of our ablation studies on HR estimation. We conduct these studies using the UCLA-rPPG dataset for intra-dataset evaluation and the UBFC-rPPG dataset for cross-dataset evaluation. Firstly, we inspect the impact of the loss function on HR estimation using our baseline model. Next, we examine the effect of video encoding by applying different CRF values to recover the

³<https://www.idiap.ch/software/bob/>

⁴https://github.com/google/mediapipe/blob/master/docs/solutions/face_mesh.md

rPPG signal within the baseline model. Finally, we evaluate the performance of our proposed training procedure.

1) Impact of loss function Before examining the impact of video compression, we conduct an analysis of the loss function in our rPPG estimator baseline model, TDM model [5]. In this initial experiment, we evaluate the performance of the TDM baseline using different loss functions: TALOS loss as a temporal loss function, SNR loss as a frequency loss function, and the proposed combination of both, from Eq. 7. Table II presents the heart rate (HR) results of our TDM baseline for each loss function in both intra- and cross-dataset evaluations.

Based on the results, we notice that the TDM model yields better HR results when trained with the TALOS loss function ($\mathcal{L}_{\text{temp}}$) as opposed to the SNR loss. However, during cross-dataset evaluation, we find that the SNR loss exhibits better generalization capabilities compared to the temporal loss. These outcomes align with the findings of Yu *et al.* [63], who highlight the challenges associated with training rPPG approaches using either temporal or spectral losses exclusively. The temporal loss offers advantages in extracting signal trend features, but it carries the risk of overfitting and limited generalization. Conversely, the SNR loss facilitates the learning of finer periodic features by leveraging the HR frequency bands. However, the presence of noise and the complexity of PPG waveforms can impede the convergence of the model. Finally, we note that the combination of both losses produces a better performance than each one individually, similarly to [60], [63]. In the intra-database, we appreciate almost the same performance combining both losses with respect to TALOS loss while in the cross-dataset evaluation, we observe a significant reduction of both MAE and RMSE compared with each of the losses individually, indicating better generalization ability. Thus, these results support our choice of the combined loss presented in Eq. 7.

2) Impact of video compression in HR estimation In

TABLE II: Impact of the loss function in HR measurement in intra-dataset and cross-dataset evaluation.

Loss function	Intra-dataset evaluation			Cross-dataset evaluation		
	UCLA-rPPG			UBFC-rPPG		
	MAE↓	RMSE↓	R↑	MAE↓	RMSE↓	R↑
$\mathcal{L}_{\text{temp}}$	1.00	4.43	0.90	2.54	6.18	0.93
$\mathcal{L}_{\text{freq}}$	1.16	4.51	0.89	2.38	5.91	0.94
$\mathcal{L}_{\text{temp}} + \mathcal{L}_{\text{freq}}$	1.02	4.45	0.90	1.66	5.54	0.95

this section, we study the impact of the H264 encoding in the recovery of the rPPG signal using our TDM baseline model. To this end, we repeat the experiments from the previous section (keeping only the combined loss) but using increasingly compressed versions of the UCLA-rPPG and UBFC-rPPG datasets. Compression is applied to the whole dataset so that there is no compression mismatch between training and test sets. Table III summarizes the HR measurement over different compression levels in terms of the CRF values.

For the intra-dataset evaluation, we observe a gradual increase in HR error as the compression rate increases. However, within the CRF range of 5 to 15, the HR error shows a rather minor increase with respect to the uncompressed baseline. On the other hand, beyond a CRF of 20, we observe a significant rise in HR error. Such CRF values correspond to about 450 kb/s, which is 4 times lower than the bit rate at CRF 15 and about 655 times lower than the uncompressed video. The observed trend coincides with previous findings, which showed significant degradation of the rPPG signal beyond this CRF value, especially when the facial videos are downsampled [49].

In contrast to the intra-database evaluation, the cross-dataset evaluation shows a substantial increase in HR error, even for the smallest CRF levels. This indicates that while the TDM baseline performs well with medium compression levels within the same database, it struggles to generalize effectively to different types of data, even when using the same compression

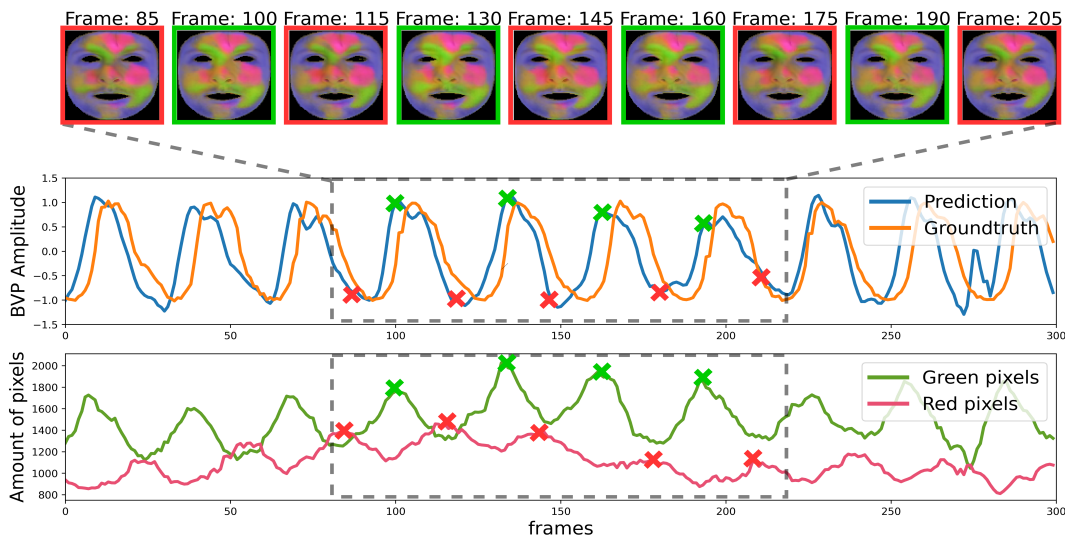


Fig. 2: Visualization of the learned video transformation for a sample compressed at CRF 15 from the UCLA-rPPG dataset. The top section displays the generated frames between frames 80 and 210. In the middle, we see the predicted rPPG and ground-truth signals. The bottom section shows the number of pixels over time for green and magenta colors, which are the dominant ones after the transformation and capture the blood pulse effect (see also the [supplementary video](#)).

TABLE III: Impact of video compression for rPPG recovery in intra-dataset and cross-dataset evaluation.

CRF	Intra-dataset evaluation			Cross-dataset evaluation		
	UCLA-rPPG			UBFC-rPPG		
	MAE↓	RMSE↓	R↑	MAE↓	RMSE↓	R↑
0	1.02	4.45	0.90	1.66	5.54	0.95
5	1.12	4.52	0.90	3.14	7.26	0.91
10	1.18	4.58	0.89	4.57	12.33	0.77
15	1.26	4.69	0.89	6.75	14.74	0.71
20	1.94	7.25	0.76	12.82	21.83	0.49
25	2.98	9.33	0.72	14.44	24.5	0.43

level as the training set. This limitation can be attributed to the TDM model primarily capturing intrinsic temporal cues of rPPG through temporal derivatives, which are more sensitive to compression artifacts in the presence of varying conditions in new testing data, such as motion or illumination. Nevertheless, to the best of our knowledge, we are the first to report cross-dataset experiments to test the effect of different compression levels, hence this limitation may not be exclusive of the TDM model but shared by other data-driven methods as well.

3) Impact of network training procedure

We conduct an evaluation of the training procedure using two different strategies: *i*) the proposed two-stage training, and *ii*) end-to-end training. Differently from the previous two sections, in which only the TDM module was used, we now incorporate also the Pulse-Signal Magnification network, thus deploying our full system.

Figure 3 depicts the evolution of HR errors using both strategies for the UCLA-rPPG and UBFC-rPPG datasets as a function of the compression level. When comparing the two strategies, it is evident that both yield competitive outcomes. However, the two-stage strategy demonstrates a lower HR error in both evaluations. Specifically, within the CRF range of 0 to 20, the two-stage procedure significantly reduces HR error compared to the end-to-end framework. This reduction helps mitigate compression degradation and achieves results similar to the uncompressed scenario. On the other hand, when the CRF is set to 25, both strategies experience an increase in HR error for both intra- and cross-dataset evaluation and their performance.

The superiority of the two-stage strategy in HR estimation, compared to end-to-end training, can be explained by various factors. In the end-to-end strategy, the network aims to recover the rPPG without any constraints related to the physiological nature of the signal. This lack of constraints increases the risk of overfitting since the system must train a larger number of parameters at the same time and the function learned by each of the two composing blocks is not necessarily the one expected by design. In contrast, the two-stage strategy employs a pre-trained TDM network that operates on uncompressed videos. This approach facilitates the learning of a video transformation that focuses solely on extracting the rPPG signal and directs attention exclusively to the regions of interest for rPPG. Hence, this initial training phase serves as a regularizer for the Pulse-Signal Magnification network, ensuring pulse-signal magnification of the input data for extracting rPPG under

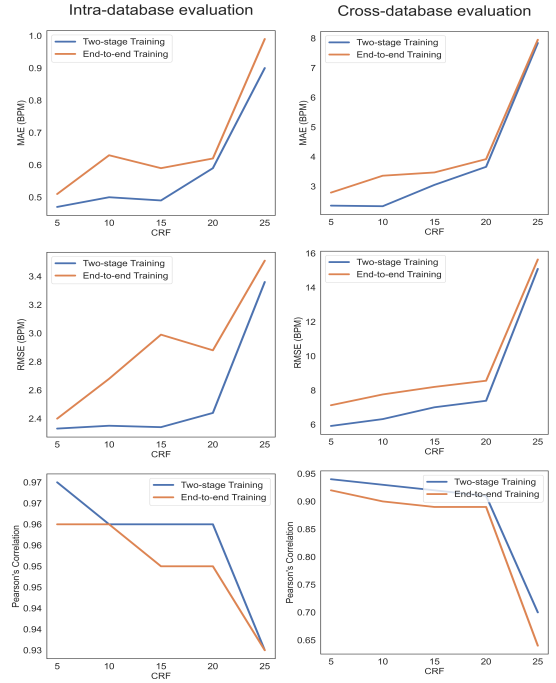


Fig. 3: Training procedure evaluation for rPPG recovery in intra-dataset and cross-dataset evaluation.

suitable conditions similar to the initial pre-trained dataset.

Independently of the training strategy, we can also analyze the impact of the Pulse-Signal Magnification block by comparing the results in Figure 3 to those from Table III. Concretely, when utilizing our Pulse-Signal Magnification network, we notice its effective stabilization of the HR error within the CRF range of 0 to 20, even for the cross-dataset evaluation, which was not the case when using just the TDM model. Beyond a CRF of 25, the HR error increases considerably, but it remains notably lower than the errors for the same CRF but without the Pulse-Signal Magnification network shown in Table III.

To gain a deeper understanding of the behavior of our proposed training framework, Figure 2 provides a detailed example of the rPPG estimation using the two-stage strategy. The visualization reveals that the Pulse-Signal Magnification network is learning a latent pulse magnification video transformation that emphasizes the facial regions relevant to rPPG extraction. Within this learned transformation, we can identify two prominent colors: green and magenta. These colors are predominantly distributed around the cheeks and forehead regions. Additionally, both in the generated video frames and the pixel evolution graph at the bottom of the figure, we can observe that the network learns opposing pulse rate patterns using these two colors which are correlated to the cardiac cycle. Specifically, green regions are primarily activated during the systolic phase, whereas magenta regions are predominantly present during the diastolic stage.

4) COHFACE and MAHNOB-HCI Datasets

After evaluating the training procedure on our ablation datasets, we also examine the impact of each training process on two highly compressed datasets: MAHNOB-HCI and COHFACE. Similar to the previous sections, we utilize both cross-database and intra-database testing protocols.

For cross-database evaluation, we train on the UCLA-rPPG dataset compressed at equivalent compression rates as the testing datasets. Specifically, for the MAHNOB-HCI dataset we use the H.264 codec with a constant bit rate of 4200 kb/s while for the COHFACE dataset, we use the MPEG-4 codec with a constant bit rate of 250 kb/s. After compressing the UCLA-rPPG dataset, we train our proposed method using this compressed dataset and directly test on the MAHNOB-HCI and COHFACE datasets.

For intra-database evaluation in MAHNOB-HCI, we start from our pre-trained model from the compressed UCLA-rPPG dataset at 4200 kb/s and fine-tune it on the MAHNOB-HCI, following the subject-independent 9-fold cross-validation protocol introduced by Yu et al. [62]. Since there is no PPG signal for this dataset, we perform the fine-tuning considering just the SNR loss, which only requires HR estimates.

For intra-database evaluation in COHFACE, we start from our pre-training model from the compressed UCLA-rPPG dataset at 250 kb/s and fine-tune it on the COHFACE using its standard partition protocol [14]. Unlike the MAHNOB-HCI dataset, COHFACE contains PPG ground-truth data, allowing us to use the combined loss function introduced in Eq. 7.

Table IV summarizes the results. Firstly, we observe that the HR errors in the intra-dataset settings are excellent for both datasets, with the two-stage training slightly outperforming the end-to-end training on MAHNOB-HCI and more clearly in COHFACE. As will be shown in Subsection IV-D, the achieved HR errors are the best ones reported for these datasets to date, showing the effectiveness of the proposed approach.

On the other hand, the cross-database errors are comparatively higher, but still at the top performance reported in comparable settings. For MAHNOB-HCI, we appreciate how two-stage training is superior to an end-to-end framework as a result of its regularization effect using the frozen TDM model pre-trained with uncompressed facial videos. Nevertheless, this does not hold for the COHFACE dataset, in which neither of the strategies performs well in the cross-database setting, possibly due to the different conditions between the UCLA-rPPG dataset and the COHFACE dataset. Additionally, the bit rate of the COHFACE dataset, which is approximately 250 kb/s, poses challenges for the recovery of the rPPG signal due to its significant degradation.

Thus, we see that the fine-tuning process shows remarkable outcomes in both datasets, demonstrating the ability of the Pulse-Signal Magnification network to fine-tune the transformation of the input video to the characteristics of the targeted database. Particularly, the two-stage strategy exhibits

TABLE IV: Training procedure evaluation for rPPG existing databases in intra-database and cross-database evaluation.

Eval	Strategy	MAHNOB-HCI			COHFACE		
		MAE↓	RMSE↓	R↑	MAE↓	RMSE↓	R↑
Cross-Database	Two-stage	3.66	5.25	0.91	10.42	17.43	-0.07
	End-to-end	5.57	7.00	0.90	10.12	17.19	-0.04
Intra-Database	Two-stage	2.40	3.37	0.94	0.70	1.53	0.98
	End-to-end	2.41	3.49	0.93	0.86	2.66	0.96

TABLE V: Results of average HR estimation of MAHNOB-HCI.

Method	Cross-dataset eval			Intra-dataset eval		
	MAE↓	RMSE↓	R↑	MAE↓	RMSE↓	R↑
Poh2011 [41]	-	13.6	0.36	-	-	-
CHROM [8]	13.49	22.36	0.2	-	-	-
Li2014 [23]	-	7.62	0.81	-	-	-
SAMC [55]	4.96	6.23	0.83	-	-	-
HR-CN [50]	-	-	-	7.25	9.24	0.51
DeepPhys [4]	4.57	6.44	0.84	-	-	-
RhythmNet [33]	-	8.28	0.64	-	3.99	0.87
STVEN+rPPGNet [62]	-	-	-	4.03	5.93	0.88
STMap+CNN [47]	5.98	7.45	0.75	4.61	5.70	0.86
AutoHR [60]	-	-	-	3.78	5.10	0.86
Meta-rPPG [19]	-	-	-	3.01	3.68	0.85
PulseGAN [46]	4.15	6.53	0.71	-	-	-
rPPG-FuseNet [17]	-	-	-	2.08	3.41	0.92
PhysFormer++ [63]	-	-	-	3.23	3.88	0.87
Proposed method	3.66	5.25	0.91	2.40	3.37	0.94

impressive results on the COHFACE database, with 0.70 BPM (Beats Per Minute) MAE, 1.53 BPM RMSE, and 0.98 Pearson’s Correlation. These findings align well with the trends depicted in Figure 3, where intra-database results demonstrate competitive even at a CRF of 25, which is approximately equivalent to a bit rate of 250 kb/s used to encode COHFACE.

D. Comparison with existing methods

To verify the generalization of our approach, we compare our results to those reported by other methods on the COHFACE and MAHNOB-HCI datasets, which are two widely used benchmarks in HR measurement with high compression rates.

1) Evaluation on MAHNOB-HCI dataset

Table V gathers the results reported in the literature for this database, separating them into intra- and cross-database to allow for a fair comparison. In terms of cross-database evaluation, our novel two-stage training procedure achieves the best results, with a MAE of 3.66 BPM and an RMSE of 5.25 BPM, outperforming handcrafted methods and all deep learning approaches that reported results in cross-database settings. Furthermore, our results outperform some learning-based approaches directly trained on the MAHNOB-HCI dataset, highlighting the ability of our model to handle data that significantly differs from the training set. The ability of our model to generalize can be attributed to our two-stage training procedure. This approach allows the Pulse-signal Magnification network to learn an appropriate transformation for accurate rPPG estimation. By incorporating the TDM module, we ensure that the learning process is constrained, preventing the model from overfitting while effectively extracting significant rPPG features.

TABLE VI: Results of average HR estimation of COHFACE.

Method	MAE↓	RMSE↓	R↑
CHROM [8]	7.8	12.45	0.26
LiCVPR [23]	19.98	25.59	-0.44
Two stream [59]	8.09	9.96	0.40
HR-CNN [50]	8.1	10.8	0.29
Tsou2020 [54]	0.68	1.65	0.72
ETA-rPPGNet [16]	4.67	6.65	0.77
Gideon2021 [11]	1.5	4.6	0.90
TFA-PFE [21]	1.31	3.92	-
TDM [5]	2.48	5.90	0.81
Proposed method	0.70	1.53	0.98

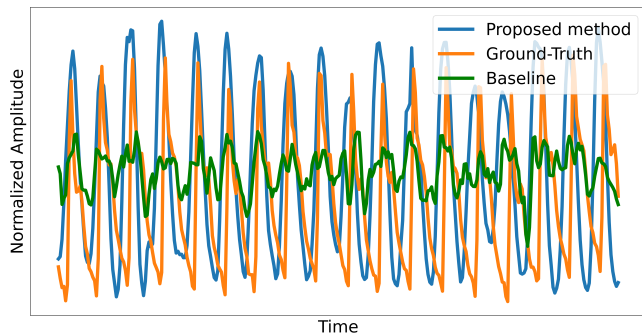


Fig. 4: Comparison of rPPG estimations between our baseline (green) and proposed model (blue) in the COHFACE dataset.

After fine-tuning our model with the MAHNOB-HCI dataset, we have observed a notable improvement in our cross-dataset results. The HR error has been reduced to 2.40 BPM for MAE, 3.37 for RMSE, and 0.94 for Pearson’s correlation. These fine-tuning results also outperform the current state-of-the-art approaches, particularly in terms of RMSE and R. It is worth noting that only the method proposed in [17], which incorporates a color space fusion technique to eliminate illumination artifacts, achieved similar results to ours, with slightly better MAE but slightly worse RMSE and R.

2) Evaluation on COHFACE dataset

The HR estimation results of the COHFACE dataset for existing methods using intra-dataset evaluation are presented in Table VI. Our method shows impressive robustness to compression and illumination conditions by adapting the learning video transformation to the dataset particularities. Table VI illustrates how fine-tuning our TDM model has achieved comparable performance to state-of-the-art methods, although certain approaches like [11], [16], [21] have achieved lower MAE and RMSE values in the test set. Nevertheless, our Pulse-Signal Magnification network adaptation and the adoption of our two-stage framework show similar HR MAE (0.70) as the siamese-rPPG approach [54] but exhibit better RMSE (1.53 BPM) value and a higher R of approximately 0.98.

The effectiveness of our proposed two-stage framework, along with the incorporation of the Pulse-Signal Magnification network, is clearly demonstrated in Figure 4. This figure presents a comparison between our TDM baseline model and our proposed approach, using the ground-truth PPG signal from a challenging COHFACE sample under challenging illumination conditions. The results highlight how the Pulse-Signal Magnification approach significantly enhances the reliability and accuracy of the rPPG signal, surpassing the performance of our TDM baseline model.

V. CONCLUSIONS

In this paper, we present a novel two-stage framework designed to mitigate the impact of video compression on remote heart measurement by employing a pulse-signal magnification video domain enhancement. Our proposed model consists of two sub-networks: an rPPG estimator and a Pulse-Signal Magnification network. We train the model using a two-stage training strategy that specifically addresses video compression

from the perspective of rPPG. In the first stage, we train the rPPG estimator using uncompressed facial videos to preserve high-quality rPPG features. In the second stage, we freeze the trained rPPG estimator and utilize it as a regularization term to guide the learning of a video transformation process for rPPG recovery. Through experiments on UCLA-rPPG and UBFC-rPPG, using intra-database and cross-database evaluations, we demonstrate the robustness of our proposed model to deal with video compression in the recovery of rPPG signal. Later, we evaluate our proposed two-stage framework using two existing highly compressed datasets, MAHNOB-HCI and COHFACE, outperforming current state-of-the-art methods. In our future work, we aim to explore the integration of a dynamic module to facilitate the adaptation of our Pulse-Signal Magnification network learning process according to the compression level of facial data.

ACKNOWLEDGMENTS

This work is partly supported by the eSCANFace project (PID2020-114083GB-I00) funded by the Spanish Ministry of Science and Innovation.

REFERENCES

- [1] Y. Benezeth, P. Li, R. Macwan, K. Nakamura, R. Gomez, and F. Yang. Remote heart rate variability for emotional state monitoring. In *EMBS Int. Conf. Biomed. Health Inform. BHI*, pages 153–156. IEEE, 2018. 1
- [2] S. Bobbia, R. Macwan, Y. Benezeth, A. Mansouri, and J. Dubois. Un-supervised skin tissue segmentation for remote photoplethysmography. *Pattern Recognit. Lett.*, 124:82–90, 2019. 2, 4, 7
- [3] L. Cerina, L. Iozzia, and L. Mainardi. Influence of acquisition frame-rate and video compression techniques on pulse-rate variability estimation from vppg signal. *Biomed Tech (Berl)*, 64(1):53–65, 2019. 1, 3
- [4] W. Chen and D. McDuff. Deepphys: Video-based physiological measurement using convolutional attention networks. In *ECCV*, pages 349–365, 2018. 2, 7, 10
- [5] J. Comas, A. Ruiz, and F. Sukno. Efficient remote photoplethysmography with temporal derivative modules and time-shift invariant loss. In *CVPR*, pages 2182–2191, 2022. 2, 5, 6, 8, 10
- [6] L. Dall’Olio, N. Curti, D. Remondini, Y. Safi Harb, F. W. Asselbergs, G. Castellani, and H.-W. Uh. Prediction of vascular aging based on smartphone acquired ppg signals. *Scientific reports*, 10:1–10, 2020. 7
- [7] A. Dasari, S. K. A. Prakash, L. A. Jeni, and C. S. Tucker. Evaluation of biases in remote photoplethysmography methods. *NPJ digital medicine*, 4(1):91, 2021. 2, 4
- [8] G. De Haan and V. Jeanne. Robust pulse rate from chrominance-based rppg. *IEEE Trans. Biomed. Eng.*, 60(10):2878–2886, 2013. 2, 6, 10
- [9] C. Dong, Y. Deng, C. C. Loy, and X. Tang. Compression artifacts reduction by a deep convolutional network. In *ICCV*, pages 576–584, 2015. 1
- [10] J. R. Estep, E. B. Blackford, and C. M. Meier. Recovering pulse rate during motion artifact with a multi-imager array for non-contact imaging photoplethysmography. In *IEEE Trans. Syst. Man Cybern. Syst.*, pages 1462–1469. IEEE, 2014. 2, 4
- [11] J. Gideon and S. Stent. The way to my heart is through contrastive learning: Remote photoplethysmography from unlabelled video. In *ICCV*, pages 3995–4004, 2021. 10, 11
- [12] A. Gudi, M. Bittner, and J. van Gemert. Real-time webcam heart-rate and variability estimation with clean ground truth for evaluation. *Applied Sciences*, 10(23):8630, 2020. 3, 4
- [13] S. Hanfland and M. Paul. Video format dependency of ppgi signals. In *Int. Conf. Electr. Eng. Inform. Commun. Technol.*, volume 1, 2016. 3
- [14] G. Heusch, A. Anjos, and S. Marcel. A reproducible study on remote heart rate measurement. *arXiv preprint arXiv:1709.00962*, 2017. 2, 4, 7, 10
- [15] G.-S. Hsu, A. Ambikapathi, and M.-S. Chen. Deep learning with time-frequency representation for pulse estimation from facial videos. In *IJCB*, pages 383–389. IEEE, 2017. 4

- [16] M. Hu, F. Qian, D. Guo, X. Wang, L. He, and F. Ren. Eta-rppgnet: Effective time-domain attention network for remote heart rate measurement. *IEEE Trans. Instrum. Meas.*, 70:1–12, 2021. **10, 11**
- [17] K. B. Jaiswal and T. Meenpal. rppg-fusenet: Non-contact heart rate estimation from facial video via rgb/msr signal fusion. *Biomed. Signal Process. Control*, 78:104002, 2022. **10, 11**
- [18] Y. Kartynnik, A. Ablavatski, I. Grishchenko, and M. Grundmann. Real-time facial surface geometry from monocular video on mobile gpus. *arXiv preprint arXiv:1907.06724*, 2019. **7**
- [19] E. Lee, E. Chen, and C.-Y. Lee. Meta-rppg: Remote heart rate estimation using a transductive meta-learner. In *ECCV*, pages 392–409. Springer, 2020. **2, 7, 10**
- [20] M. Lewandowska, J. Rumiński, T. Kocejko, and J. Nowak. Measuring pulse rate with a webcam—a non-contact method for evaluating cardiac activity. In *FedCSIS*, pages 405–410. IEEE, 2011. **2**
- [21] J. Li, Z. Yu, and J. Shi. Learning motion-robust remote photoplethysmography through arbitrary resolution videos. In *AAAI*, volume 37, pages 1334–1342, 2023. **10, 11**
- [22] X. Li, I. Alikhani, J. Shi, T. Seppanen, J. Juntila, K. Majamaa-Voltti, M. Tulppo, and G. Zhao. The obf database: A large face video database for remote physiological signal measurement and atrial fibrillation detection. In *FG*, pages 242–249. IEEE, 2018. **2, 4**
- [23] X. Li, J. Chen, G. Zhao, and M. Pietikainen. Remote heart rate measurement from face videos under realistic situations. In *CVPR*, pages 4264–4271, 2014. **2, 10**
- [24] S. Liu, P. C. Yuen, S. Zhang, and G. Zhao. 3d mask face anti-spoofing with remote photoplethysmography. In *ECCV*, pages 85–100. Springer, 2016. **1**
- [25] X. Liu, B. Hill, Z. Jiang, S. Patel, and D. McDuff. Efficientphys: Enabling simple, fast and accurate camera-based cardiac measurement. In *IEEE Winter Conf. Appl. Comput. Vis.*, pages 5008–5017, 2023. **2**
- [26] X. Liu, Z. Jiang, J. Fromm, X. Xu, S. Patel, and D. McDuff. Metaphys: few-shot adaptation for non-contact physiological measurement. In *CHIL*, pages 154–163, 2021. **2**
- [27] H. Lu, H. Han, and S. K. Zhou. Dual-gan: Joint bvp and noise modeling for remote physiological measurement. In *CVPR*, pages 12404–12413, 2021. **2**
- [28] E. Magdalena Nowara, T. K. Marks, H. Mansour, and A. Veeraraghavan. Sparseppg: Towards driver monitoring using camera-based vital signs estimation in near-infrared. In *CVPRW*, pages 1272–1281, 2018. **2, 4**
- [29] D. McDuff. Deep super resolution for recovering physiological information from videos. In *CVPRW*, pages 1367–1374, 2018. **3**
- [30] D. J. McDuff, E. B. Blackford, and J. R. Estep. The impact of video compression on remote cardiac pulse measurement using imaging photoplethysmography. In *FG*, pages 63–70. IEEE, 2017. **1, 3, 7**
- [31] X. Niu, H. Han, S. Shan, and X. Chen. Synrhythm: Learning a deep heart rate estimator from general to specific. In *ICPR*, pages 3580–3585. IEEE, 2018. **2**
- [32] X. Niu, H. Han, S. Shan, and X. Chen. Vipl-hr: A multi-modal database for pulse estimation from less-constrained face video. In *ACCV*, pages 562–576. Springer, 2018. **2, 3**
- [33] X. Niu, S. Shan, H. Han, and X. Chen. Rhythmnet: End-to-end heart rate estimation from face via spatial-temporal representation. *IEEE TIP*, 29:2409–2423, 2019. **2, 4, 10**
- [34] E. Nowara and D. McDuff. Combating the impact of video compression on non-contact vital sign measurement using supervised learning. In *ICCVW*, pages 0–0, 2019. **1, 3, 5**
- [35] E. M. Nowara, D. McDuff, and A. Veeraraghavan. The benefit of distraction: Denoising camera-based physiological measurements using inverse attention. In *ICCV*, pages 4955–4964, 2021. **2**
- [36] E. M. Nowara, D. McDuff, and A. Veeraraghavan. Systematic analysis of video-based pulse measurement from compressed videos. *Biomed. Opt. Express*, 12(1):494–508, 2021. **1, 3**
- [37] A. Pai, A. Veeraraghavan, and A. Sabharwal. Hrvcam: robust camera-based measurement of heart rate variability. *J. Biomed. Opt.*, 26(2):022707–022707, 2021. **4**
- [38] A. Paszke, S. Gross, F. Massa, A. Lerer, J. Bradbury, G. Chanan, T. Killeen, Z. Lin, N. Gimelshein, L. Antiga, et al. Pytorch: An imperative style, high-performance deep learning library. *Adv Neural Inf Process Syst*, 32, 2019. **7**
- [39] O. Perepelkina, M. Artemyev, M. Churikova, and M. Grinenko. Heart-track: Convolutional neural network for remote video-based heart rate monitoring. In *CVPRW*, pages 288–289, 2020. **2, 4**
- [40] M.-Z. Poh, D. J. McDuff, and R. W. Picard. Advancements in non-contact, multiparameter physiological measurements using a webcam. *IEEE Trans. Biomed. Eng.*, 58(1):7–11, 2010. **2**
- [41] M.-Z. Poh, D. J. McDuff, and R. W. Picard. Non-contact, automated cardiac pulse measurements using video imaging and blind source separation. *Optics express*, 18(10):10762–10774, 2010. **2, 10**
- [42] M. Rapczynski, P. Werner, and A. Al-Hamadi. Effects of video encoding on camera-based heart rate estimation. *IEEE Trans. Biomed. Eng.*, 66(12):3360–3370, 2019. **1, 3**
- [43] V. Ronca, A. Giorgi, D. Rossi, A. Di Florio, G. Di Flumeri, P. Aricò, N. Sciaraffa, A. Vozzi, L. Tamborra, I. Simonetti, et al. A video-based technique for heart rate and eye blinks rate estimation: A potential solution for telemonitoring and remote healthcare. *Sensors*, 21(5):1607, 2021. **1**
- [44] R. M. Sabour, Y. Benezeth, P. De Oliveira, J. Chappe, and F. Yang. Ufbc-phys: A multimodal database for psychophysiological studies of social stress. *IEEE Trans. Affect. Comput.*, 2021. **2, 4**
- [45] M. Soleymani, J. Lichtenauer, T. Pun, and M. Pantic. A multimodal database for affect recognition and implicit tagging. *IEEE Trans. Affect. Comput.*, 3(1):42–55, 2011. **2, 4, 7**
- [46] R. Song, H. Chen, J. Cheng, C. Li, Y. Liu, and X. Chen. PulseGAN: Learning to generate realistic pulse waveforms in remote photoplethysmography. *IEEE J.Biomed.Health Inform.*, 25(5):1373–1384, 2021. **2, 10**
- [47] R. Song, S. Zhang, C. Li, Y. Zhang, J. Cheng, and X. Chen. Heart rate estimation from facial videos using a spatiotemporal representation with convolutional neural networks. *IEEE Trans. Instrum. Meas.*, 69(10):7411–7421, 2020. **10**
- [48] J. Speth, N. Vance, A. Czajka, K. W. Bowyer, D. Wright, and P. Flynn. Deception detection and remote physiological monitoring: A dataset and baseline experimental results. In *IJCB*, pages 1–8. IEEE, 2021. **4**
- [49] R. Špetlík, J. Cech, and J. Matas. Non-contact reflectance photoplethysmography: Progress, limitations, and myths. In *FG*, pages 702–709. IEEE, 2018. **1, 2, 3, 8**
- [50] R. Špetlík, V. Franc, and J. Matas. Visual heart rate estimation with convolutional neural network. In *BMVC*, 2018. **2, 4, 10**
- [51] R. Stricker, S. Müller, and H.-M. Gross. Non-contact video-based pulse rate measurement on a mobile service robot. In *RO-MAN*, pages 1056–1062. IEEE, 2014. **2, 4**
- [52] C. Takano and Y. Ohta. Heart rate measurement based on a time-lapse image. *Medical engineering & physics*, 29(8):853–857, 2007. **2**
- [53] H. E. Tasli, A. Gudi, and M. Den Uyl. Remote ppg based vital sign measurement using adaptive facial regions. In *ICIP*, pages 1410–1414. IEEE, 2014. **4**
- [54] Y.-Y. Tsou, Y.-A. Lee, C.-T. Hsu, and S.-H. Chang. Siamese-rppg network: remote photoplethysmography signal estimation from face videos. In *Proc.ACM Symp.Appl.Comput.*, pages 2066–2073, 2020. **10, 11**
- [55] S. Tulyakov, X. Alameda-Pineda, E. Ricci, L. Yin, J. F. Cohn, and N. Sebe. Self-adaptive matrix completion for heart rate estimation from face videos under realistic conditions. In *CVPR*, pages 2396–2404, 2016. **2, 10**
- [56] W. Verkrusse, L. O. Svaasand, and J. S. Nelson. Remote plethysmographic imaging using ambient light. *Optics express*, 16(26):21434–21445, 2008. **2**
- [57] W. Wang, S. Stuijk, and G. De Haan. A novel algorithm for remote photoplethysmography: Spatial subspace rotation. *IEEE Trans. Biomed. Eng.*, 63(9):1974–1984, 2015. **2**
- [58] Z. Wang, Y. Ba, P. Chari, O. D. Bozkurt, G. Brown, P. Patwa, N. Vaddi, L. Jalilian, and A. Kadambi. Synthetic generation of face videos with plethysmograph physiology. In *CVPR*, pages 20587–20596, 2022. **2, 4, 6**
- [59] Z.-K. Wang, Y. Kao, and C.-T. Hsu. Vision-based heart rate estimation via a two-stream cnn. In *ICIP*, pages 3327–3331. IEEE, 2019. **10**
- [60] Z. Yu, X. Li, X. Niu, J. Shi, and G. Zhao. Autohr: A strong end-to-end baseline for remote heart rate measurement with neural searching. *IEEE Sign. Process. Letters*, 27:1245–1249, 2020. **8, 10**
- [61] Z. Yu, X.-B. Li, and G. Zhao. Remote photoplethysmograph signal measurement from facial videos using spatio-temporal networks. In *BMVC*, 2019. **2**
- [62] Z. Yu, W. Peng, X. Li, X. Hong, and G. Zhao. Remote heart rate measurement from highly compressed facial videos: an end-to-end deep learning solution with video enhancement. In *ICCV*, pages 151–160, 2019. **1, 2, 3, 7, 10**
- [63] Z. Yu, Y. Shen, J. Shi, H. Zhao, Y. Cui, J. Zhang, P. Torr, and G. Zhao. Physformer++: Facial video-based physiological measurement with slowfast temporal difference transformer. *IJCV*, 131(6):1307–1330, 2023. **2, 8, 10**

- [64] K. Zhang, W. Zuo, Y. Chen, D. Meng, and L. Zhang. Beyond a gaussian denoiser: Residual learning of deep cnn for image denoising. *IEEE TIP*, 26(7):3142–3155, 2017. [1](#)
- [65] Z. Zhang, J. M. Girard, Y. Wu, X. Zhang, P. Liu, U. Ciftci, S. Canavan, M. Reale, A. Horowitz, H. Yang, et al. Multimodal spontaneous emotion corpus for human behavior analysis. In *CVPR*, pages 3438–3446, 2016. [2](#), [4](#)
- [66] C. Zhao, W. Chen, C.-L. Lin, and X. Wu. Physiological signal preserving video compression for remote photoplethysmography. *IEEE Sens. J.*, 19(12):4537–4548, 2019. [1](#), [3](#)
- [67] C. Zhao, C.-L. Lin, W. Chen, and Z. Li. A novel framework for remote photoplethysmography pulse extraction on compressed videos. In *CVPRW*, pages 1299–1308, 2018. [1](#), [3](#)